Scripta Materialia 220 (2022) 114936

Contents lists available at ScienceDirect

Scripta Materialia

journal homepage: www.journals.elsevier.com/scripta-materialia

Mechanical properties of hexagonal silicon

Tao Liang [a,b], Lianghua Xiong [c], Hongbo Lou [b], Fujun Lan [b], Junran Zhang [d], Ye Liu [b], Dongsheng Li [e], Qiaoshi Zeng [b,*], Zhidan Zeng [b,*]

[a] Jiangsu Key Laboratory of Advanced Metallic Materials, School of Materials Science and Engineering, Southeast University, Nanjing 211189, China
[b] Center for High Pressure Science and Technology Advanced Research, Shanghai 201203, China
[c] Shanghai Key Lab of Advanced High-temperature Materials and Precision Forming, School of Materials Science and Engineering, Shanghai Jiao Tong University, Shanghai 200240, China
[d] Hangzhou Global Scientific and Technological Innovation Center, Zhejiang University, Hangzhou 311200, China
[e] State Key Laboratory of Silicon Materials and School of Materials Science and Engineering, Zhejiang University, Hangzhou 310027, China

ARTICLE INFO

Keywords:
Silicon
Mechanical properties
Synchrotron radiation
X-ray diffraction
Nanoindentation

ABSTRACT

Hexagonal silicon (Si-IV) has recently attracted considerable research interest due to its extraordinary optical properties and possibility to convert into a direct semiconductor under strain with great potential for applications. However, the mechanical properties of Si-IV, which are critical for its applications, have not been experimentally studied yet. In this study, combining nanoindentation and *in situ* high-pressure synchrotron X-ray diffraction, we thoroughly investigated the mechanical properties of Si-IV. The results suggest that the elastic moduli and hardness of Si-IV are close to those of the common diamond cubic silicon. The similar mechanical properties of Si-IV and diamond cubic silicon are beneficial for integrating Si-IV into conventional Si-based devices using similar industrial processing and for its photovoltaic and optoelectronic applications.

Hexagonal silicon (Si-IV, also known as lonsdaleite or wurtzite Si) has attracted considerable research interest recently due to its extraordinary optical properties and potential key role in Si-based optoelectronics and photovoltaics [1–7]. Si-IV shows a remarkable enhancement in light absorption in the visible range compared with that of the common diamond cubic silicon [4,5]. In addition, it has strong photoluminescence emission in the visible region, with the emission peak centered around 750 nm [4,5]. More interestingly, a*b initio* calculations suggest that the indirect bandgap of Si-IV would convert to a direct bandgap with strain [6]. Furthermore, tunable direct bandgaps were achieved by introducing Ge to form various hexagonal SiGe alloys [8]. The hexagonal SiGe alloys show light emission with continuously changed wavelength over a broad range, with emission yield comparable to direct bandgap III-V semiconductors. Therefore, it would be possible to unite electronic and optoelectronic functionalities on a single chip [8].

Although Si-IV has been obtained by chemical vapor deposition or epitaxial growth on gallium phosphide nanowires [7,9], synthesizing pure Si-IV through chemical reactions is quite challenging. [4] Fortunately, Si-IV can also be synthesized through solid-state phase transitions under high pressure [4,10–12]. The common diamond cubic silicon (Si-I) transforms to a β-Sn phase when compressed to ~ 12 GPa, and the β-Sn phase would transform to body-centered cubic silicon (Si-III) after full release of pressure through an intermediate rhombohedral phase (Si-XII) [13–16]. Phase pure Si-IV can then be achieved by annealing the Si-III at 200–600 °C [4,11]. In addition, another study found that pure hexagonal silicon could also be synthesized by heating a recently discovered Si_{24} allotrope [1]. Despite many theoretical studies, the structure and many basic properties of Si-IV are still not well-explored experimentally due to the difficulties in the synthesis of pure Si-IV [2–4,6]. For instance, recent synchrotron X-ray diffraction (XRD) and transmission electron microscopy studies suggest that Si-IV has a 4*H* structure instead of a 2*H* structure [1,4]. Due to the challenges in measuring the mechanical properties of tiny samples synthesized under high pressure, the mechanical properties of Si-IV, which are crucial for its future applications, have not been experimentally studied yet.

In this study, we utilized high pressure to synthesize pure Si-IV and then combined *in situ* high-pressure synchrotron X-ray diffraction (XRD) and nanoindentation technique to determine Young's modulus, bulk modulus, and hardness of Si-IV. The shear modulus and Poisson's ratio were then calculated based on the experimental results. The results

* Corresponding authors.
E-mail addresses: zengqs@hpstar.ac.cn (Q. Zeng), zengzd@hpstar.ac.cn (Z. Zeng).

https://doi.org/10.1016/j.scriptamat.2022.114936
Received 20 April 2022; Received in revised form 9 July 2022; Accepted 17 July 2022
Available online 22 July 2022

would provide essential information for designing and developing novel silicon devices based on Si-IV in the future.

Bulk Si-IV samples were firstly synthesized through high-pressure and high-temperature treatment on Si-I. Specifically, a Si-I flake (~50 μm thick) was loaded in a symmetrical diamond anvil cell (DAC) together with tiny ruby balls as the pressure calibrant [17]. Methanol-ethanol mixture (volume ratio of 4:1) was used as the pressure transmitting medium for all the high-pressure experiments [18]. The Si-I sample was compressed to 16~20 GPa at room temperature, followed by decompression to ambient pressure. The recovered sample was then removed from the DAC for annealing at 300°C for 30 min in a pure Ar atmosphere. The crystal structure of the synthesized Si-IV sample was checked by synchrotron XRD at the beamline 15U1 of Shanghai Synchrotron Radiation Facility (SSRF), with a focused X-ray beam with size of 3 μm ×3 μm and a wavelength of 0.6199 Å. Two dimensional diffraction images were collected using a MAR165 CCD detector and then integrated to one dimensional XRD patterns using the software Dioptas and further analyzed with GSAS-II [19,20].

Nanoindentation is a powerful and handy tool to determine the mechanical properties of tiny samples. Reliable nanoindentation measurements require firmly mounting of samples, which is critical and usually challenging for tiny samples. Therefore, a Si-IV sample (around ~50 μm thick) with flat surfaces was tightly fixed on a substrate using epoxy under a stereomicroscope for the nanoindentation tests. A (100)-oriented single-crystalline Si-I sample with a similar size was also fixed using the same approach for comparison. Nanoindentation tests were performed using KLA G200 Nano-indenter equipped with a Berkovich indenter, with the continuous stiffness measurement (CSM) technique [21]. The maximum indentation depth was 300 nm, far below 1/20 of the sample thickness, and the loading/unloading strain rate was 0.05 s^{-1}. The allowable thermal drift rate was 0.05 nm/s, and the actual thermal drift was measured and corrected at 90% unload.

One synthesized Si-IV sample was re-loaded into a symmetrical DAC for *in situ* high-pressure XRD. The experiments were performed at the beamline 13IDD of Advanced Photon Source (APS), Argonne National Laboratory (ANL), with the X-ray wavelength of 0.3344 Å and beam size of 3 μm × 4 μm. The sample chamber was a hole with a diameter of ~120 μm drilled in the center of a pre-indented (~20 GPa) rhenium gasket. Gold foil (4 μm thick) was used as the pressure calibrant, and the pressure was estimated according to the equation of state of gold [22]. The 2D diffraction images were collected using a PILATUS CdTe 1 M detector and integrated into 1D XRD patterns using the software Dioptas [20].

Fig. 1a and 1b show the optical microscope images of an initial (100)-oriented single-crystalline Si-I sample loaded in a DAC and the recovered sample after high-pressure treatment followed by annealing at 300°C, respectively. The crystal structure of the recovered sample was determined by synchrotron XRD. The initial single crystalline Si-I sample transformed into a polycrystalline phase as evidenced by the smooth powder diffraction rings shown in the inset of Fig. 1c. The XRD pattern (as shown in Fig. 1c) could be well refined (R_{wp} = 6.51%) using a hexagonal structure (space group: $P6_3/mmc$) with lattice parameters of $a = 3.815$ Å and $c = 6.348$ Å, which are consistent with previous studies and confirm the synthesized sample is purely Si-IV [11,13]. Then the density of Si-IV is estimated to be 2.324 g/cm^3, almost the same with that of Si-I (2.33 g/cm^3) considering the experimental error. It should be mentioned that, Si-IV is recently proposed to have a 4*H* structure, whose XRD is slightly different from that of a 2*H* structure [1,4]. The diffused diffraction rings and the broad XRD peaks of our sample make it rather difficult to determine whether it has a 2*H* or 4*H* structure. In this study, we mainly focused on the properties of Si-IV.

Due to the limited size of the Si-IV sample (size around or below 100 μm, thickness around 50 μm, see Fig. 1b), nanoindentation is an appropriate method to measure the hardness and Young's modulus (*E*) of the sample. Fig. 2a shows the load-displacement curve of the Si-IV sample. The curve is continuous during loading and shows a "pop-out"

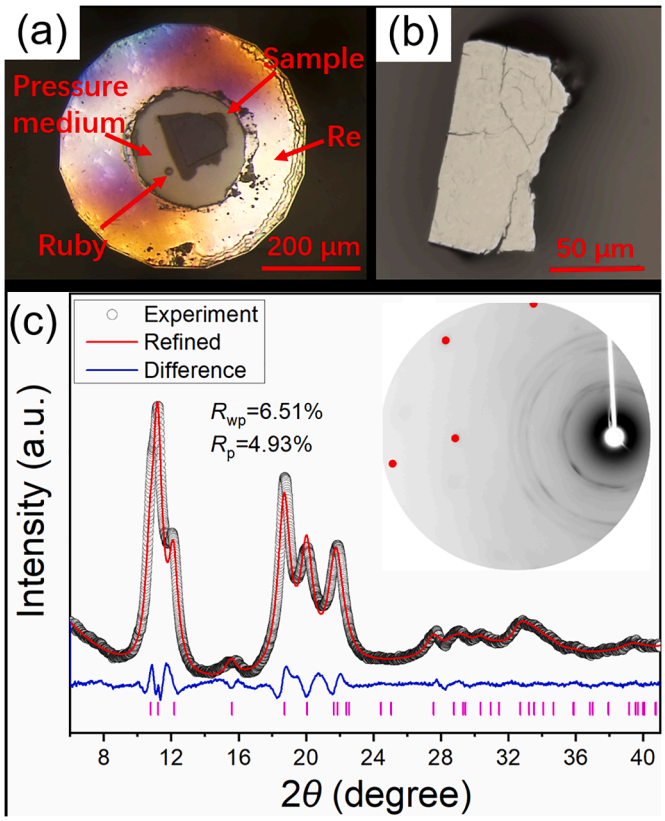

Fig. 1. (a) An optical microscope image of a single crystalline Si-I sample loaded in a DAC for high-pressure experiments. (b) An optical microscope image of the synthesized Si-IV sample. (c) The synchrotron XRD pattern of the polycrystalline Si-IV sample (black circles) at ambient conditions. The red and the blue lines represent the Rietveld refinement result and the fit residual, respectively. The X-ray wavelength was 0.6199 Å. The inset shows the 2D diffraction image of the Si-IV sample with smooth diffraction rings, and the diffraction spots from the substrate are masked (red circles).

during unloading. Pop-out has been observed in many nanoindentation experiments of Si-I [23–25]. In these nanoindentation experiments, Si-I transforms to Si-II during loading, and Si-II changes to Si-XII and/or Si-III during unloading [23,25]. The pop-out is attributed to the volume expansion associated with the Si-II → Si-XII/Si-III phase transitions. Therefore, the pop-out in the unloading curve of Si-IV might be attributed to phase transition as well. The Raman spectrum collected on the indent of Si-IV (with a loading force of ~90 mN) is consistent with that of Si-XII/Si-III phase which were observed in the indents of Si-I [23,26], implying similar phase transitions during the unloading of nanoindentation tests of Si-IV. The details of the phase transition call for further study in the future.

CSM technique was used for the nanoindentation tests during loading [21,27], and Young's modulus and hardness of these two samples as a function of displacement could be obtained (see Fig. 2b and c). Both Young's modulus and hardness are mostly constant over the 100–200 nm range, implying that the test results herein were not affected by the substrate [21]. The Young's modulus and hardness of the samples were then obtained by averaging these data. These results will be discussed later together with the bulk modulus derived from *in situ* high-pressure XRD experiments.

Fig. 3a shows the *in situ* high-pressure XRD experiments of Si-IV. All the diffraction peaks of Si-IV shift toward higher 2θ with increasing pressure, and no new peaks were observed, indicating the Si-IV phase remains stable up to 10.4 GPa. The unit cell volume of Si-IV at different pressures was determined from the refinement of the XRD patterns, and the pressure-volume data were fit to a third-order Birch-Murnaghan

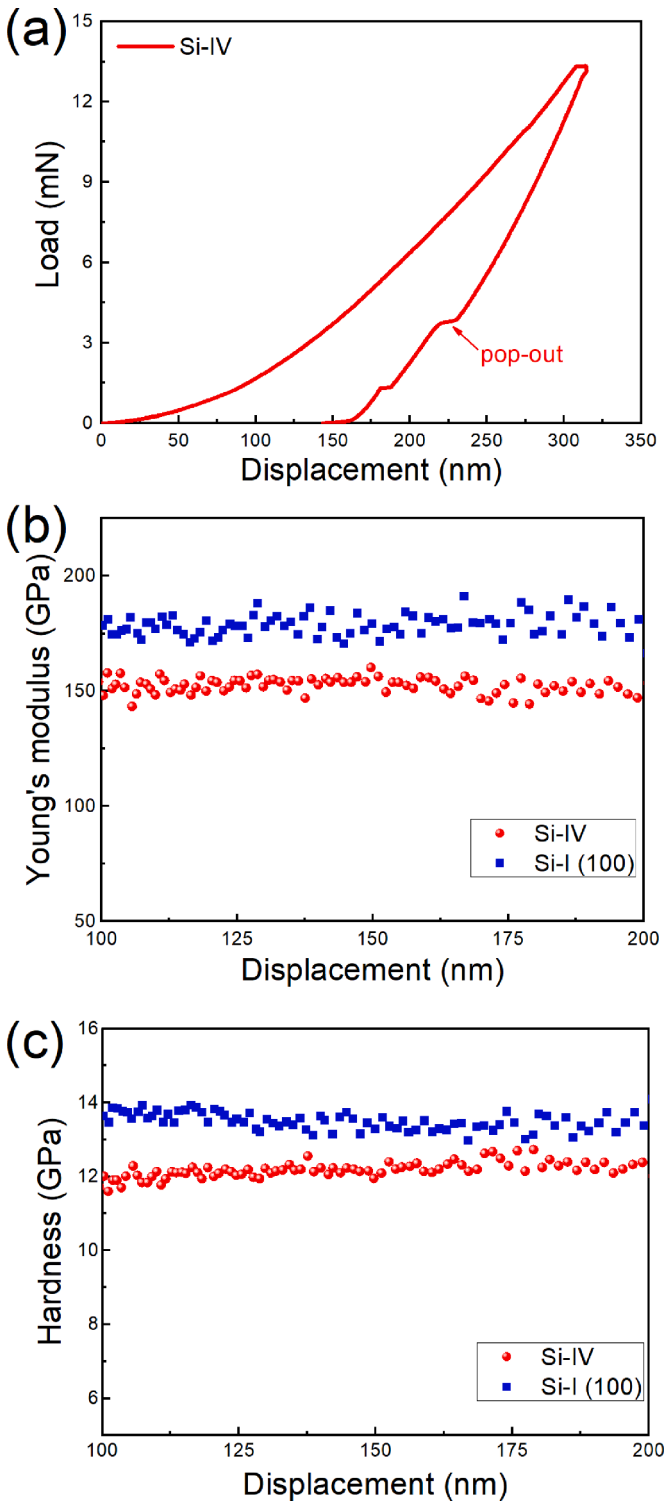

Fig. 2. (a) A representative load-displacement curve of the Si-IV sample obtained by nanoindentation experiment using CSM. The maximum indentation depth is 300 nm, and the strain rate is 0.05 s^{-1}. Young's modulus (b) and hardness (c) as functions of displacement of polycrystalline Si-IV (red circle) and (100)-oriented single-crystalline Si-I (blue square) in the range of 100 nm to 200 nm.

isothermal equation of state (BM-EOS) (see Fig. 3b) [28]. With the pressure derivative $B^{'}$ fixed at 4, the bulk modulus of Si-IV was derived from the fitting, i.e., $B_0 = 91.8 \pm 3.0$ GPa. This value is very close to the 92.8 GPa predicted in previous *ab initio* calculations [6]. The unit cell

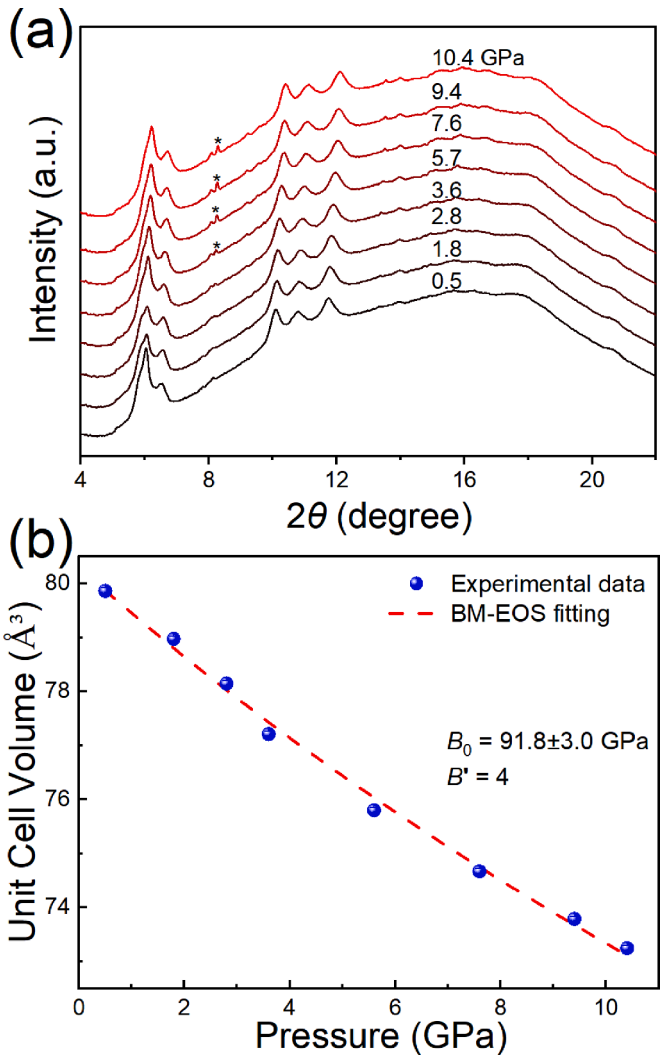

Fig. 3. (a) *In situ* high-pressure XRD patterns of Si-IV up to 10.4 GPa. (b) The unit cell volume as a function of pressure. The dashed line shows the fitting result using a third-order BM-EOS. The error bars are smaller than the symbol size. The X-ray wavelength is 0.3344 Å. The peaks from pressure standard gold are marked by the asterisk symbols.

volume at ambient pressure (V_0) derived from the EOS fitting was 80.3 ± 0.1 Å^3, which is consistent with our XRD results of Si-IV at ambient pressure (V = 80.0 Å^3) and indicates the high quality of the high-pressure XRD data.

With the bulk modulus derived from the high-pressure XRD experiments and Young's modulus determined in the nanoindentation experiments, the shear modulus (G) and Poisson's ratio (υ) can be further derived from bulk modulus (B) and Young's modulus (E) using the following relations, as the polycrystalline Si-IV can be approximated to be isotropic:

$$E = 3B(1 - 2\upsilon) \quad (1)$$

$$E = 2G(1 + \upsilon) \quad (2)$$

All the results are summarized in Table 1 in comparison with the elastic moduli and hardness of polycrystalline Si-I from the literature [6, 27,29–33]. The Young's modulus and hardness of (100) Si-I are consistent with those from previous nanoindentation studies, with the difference around or less than 5% [27,34], which is a good indicator of the reliability of our tests on tiny samples.

As shown in Table 1, all of the elastic moduli of Si-IV, including the

Table 1
Mechanical properties of Si-IV in comparison with those of Si-I, including Young's modulus (E), bulk modulus (B), hardness (H), shear modulus (G), and Poisson's ratio (υ).

Si phase	E (GPa)	B (GPa)	H (GPa)	G (GPa)	υ	Notes
Si-IV (polycrystal)	152.4 ± 3.2	91.8 ± 3.0	12.0 ± 0.2	62.3	0.22	This study
	202	92.8	–	–	0.167	Simulation [6]
Si-I (100)	178.9 ± 4.6	–	13.5 ± 0.2	–	–	This study
Si-I	169 ± 6.15	–	–	69	0.22	Exp [32].
(polycrystal)	163.0 ± 2.0	–	–	–	–	Exp [30].
	–	–	10.5 ± 1.5	–	–	Exp [31].
	181	–	12.6	–	–	Exp [29].
	–	97–101	–	–	–	Exp [33].

Note: G of polycrystalline Si-I is calculated based on E and υ.

bulk modulus, Young's modulus, and shear modulus, are only slightly lower (around or less than 10%) than those of polycrystalline Si-I. The atoms in both Si-IV and Si-I are connected through sp^3 hybridized covalent bonds. According to the Rietveld refinement results, the Si-Si bonds in Si-IV have two lengths, i.e., 2.37 Å and 2.34 Å, close to the 2.35 Å in Si-I. The similar elastic moduli of Si-IV and Si-I are reasonable given these similar features in their atomic bonds. The relatively lower elastic moduli of Si-IV can be mainly attributed to the nanometer-sized grains of the sample, which introduces a considerable amount of grain boundaries with disordered structures [35].

In addition, the hardness of polycrystalline Si-IV and Si-I are also close. The Si atoms in Si-I are connected through strong, directional covalent bonds; hence the dislocation activities in Si-I are largely inhibited at room temperature due to the high Peierls barrier, and the hardness and plastic deformation of Si-I are mainly controlled by the pressure-induced phase transitions and the ductile high-pressure phases [24,36–38]. The fact that Si-IV has a hardness close to that of Si-I implies it is also a brittle phase in which the dislocation activities are suppressed at room temperature. This is consistent with the previous discussion that the features of Si-Si bonds in Si-IV are similar to that of Si-I. As mentioned before, a pop-out was observed in the unloading curve of Si-IV. As a consequence, it can be inferred that the plasticity of Si-IV is also mainly contributed by the pressure-induced phase transition from Si-IV to a ductile phase (maybe Si-II) above critical stress.

In summary, by combining *in situ* high-pressure synchrotron XRD and nanoindentation technique, we fully investigated the mechanical properties of Si-IV. The elastic moduli, Poisson's ratio, and hardness of Si-IV were obtained from experiments for the first time, i.e., Young's modulus 152.4 ± 3.2 GPa, bulk modulus 91.8 ± 3.0 GPa, shear modulus ~62.3 GPa, Poisson's ratio ~0.223, and hardness 12.0 GPa ± 0.2 GPa. All the elastic moduli of Si-IV are slightly lower than those of Si-I, and the hardness of the two phases are quite close. Overall, the mechanical properties of Si-IV are quite similar to those of Si-I, which is beneficial for integrating Si-IV into conventional Si-based devices using similar industrial processing. These results also demonstrate the feasibility and reliability of nanoindentation tests on DAC recovered tiny samples to determine their mechanical properties. The accurately determined mechanical properties of Si-IV in this work would guide the practical applications of Si-IV in the future.

Data availability statement

The data that support the findings of this study are available from the corresponding author upon reasonable request.

Declaration of Competing Interest

The authors declare that they have no known competing financial interests or personal relationships that could have appeared to influence the work reported in this paper.

Acknowledgments

The authors acknowledge financial support from the National Key R&D Program of China (2021YFA0718900) and the National Natural Science Foundation of China (51871054). XRD experiments were performed at beamlines 13 ID-D of GeoSoilEnviroCARS, Advanced Photon Source (APS), Argonne National Laboratory (ANL), and 15U1 of Shanghai Synchrotron Radiation Facility (SSRF), China. GeoSoilEnviroCARS is supported by the National Science Foundation – Earth Sciences (EAR – 1634415) and Department of Energy- GeoSciences (DE-FG02–94ER14466). APS is supported by DOE, Office of Basic Energy Sciences (BES), under Contract No. DE-AC02–06CH11357.

References

[1] T.B. Shiell, L. Zhu, B.A. Cook, J.E. Bradby, D.G. McCulloch, T.A. Strobel, Phys. Rev. Lett. 126 (21) (2021), 215701.
[2] L. Sun, M.R.G. Marques, M.A.L. Marques, S. Botti, Phys. Rev. Mater. 5 (6) (2021), 064605.
[3] R. Kita, M. Toyoda, S. Saito, Phys. Rev. Mater. 5 (6) (2021), 063402.
[4] S. Pandolfi, C. Renero-Lecuna, Y. Le Godec, B. Baptiste, N. Menguy, M. Lazzeri, C. Gervais, K. Spektor, W.A. Crichton, O.O. Kurakevych, Nano Lett. 18 (9) (2018) 5989–5995.
[5] S. Dixit, A.K. Shukla, J. Appl. Phys. 123 (22) (2018) 224301.
[6] C. Rödl, T. Sander, F. Bechstedt, J. Vidal, P. Olsson, S. Laribi, J.F. Guillemoles, Phys. Rev. B 92 (4) (2015), 045207.
[7] H.I. Hauge, M.A. Verheijen, S. Conesa-Boj, T. Etzelstorfer, M. Watzinger, D. Kriegner, I. Zardo, C. Fasolato, F. Capitani, P. Postorino, S. Kolling, A. Li, S. Assali, J. Stangl, E.P. Bakkers, Nano Lett. 15 (9) (2015) 5855–5860.
[8] E. Fadaly, A. Dijkstra, J.R. Suckert, D. Ziss, M.V. Tilburg, C. Mao, Y. Ren, V. V. Lange, K. Korzun, S. Kling, Nature 580 (2020) 205–209.
[9] A. Fontcuberta i Morral, J. Arbiol, J.D. Prades, A. Cirera, J.R. Morante, Adv. Mater. 19 (10) (2007) 1347–1351.
[10] L.Q. Huston, A. Lugstein, G. Shen, D.A. Cullen, B. Haberl, J.S. Williams, J. E. Bradby, Nano Lett. 21 (3) (2021) 1427–1433.
[11] J.S. Kasper, R.H. Wentorf, Science 197 (4303) (1977), 599-599.
[12] B. Haberl, T.A. Strobel, J.E. Bradby, Appl. Phys. Rev. 3 (4) (2016), 040808.
[13] J.R.H. Wentorf, J.S. Kasper, Science 139 (1963) 338–339.
[14] H. Zhang, H. Liu, K. Wei, O.O. Kurakevych, Y. Le Godec, Z. Liu, J. Martin, M. Guerrette, G.S. Nolas, T.A. Strobel, Phys. Rev. Lett. 118 (14) (2017), 146601.
[15] L. Fan, D. Yang, D. Li, Materials (Basel) 14 (14) (2021) 3964.
[16] Y. Xuan, L. Tan, B. Cheng, F. Zhang, X. Chen, M. Ge, Q. Zeng, Z. Zeng, J. Phys. Chem. C 124 (49) (2020) 27089–27096.
[17] H.K. Mao, P.M. Bell, J.W. Shaner, D.J. Steinberg, J. Appl. Phys. 49 (6) (1978) 3276–3283.
[18] X. Chen, H. Lou, Z. Zeng, B. Cheng, X. Zhang, Y. Liu, D. Xu, K. Yang, Q. Zeng, Matter Radiat. at Extreme 6 (3) (2021), 038402.
[19] B.H. Toby, R.B. Von Dreele, J. Appl. Crystallogr. 46 (2) (2013) 544–549.
[20] C. Prescher, V.B. Prakapenka, High Pressure Res. 35 (3) (2015) 223–230.
[21] X. Li, B. Bhushan, Mater. Charact. 48 (1) (2002) 11–36.
[22] O.L. Anderson, D.G. Isaak, S. Yamamoto, J. Appl. Phys. 65 (4) (1989) 1534–1543.
[23] J.I. Jang, M.J. Lance, S. Wen, T.Y. Tsui, G.M. Pharr, Acta Mater. 53 (6) (2005) 1759–1770.
[24] Z. Zeng, L. Wang, X. Ma, S. Qu, J. Chen, Y. Liu, D. Yang, Scr. Mater. 64 (9) (2011) 832–835.
[25] J.E. Bradby, J.S. Williams, M.V. Swain, Phys. Rev. B 67 (8) (2003), 085205.
[26] Z. Zeng, Q. Zeng, W.L. Mao, S. Qu, J. Appl. Phys. 115 (10) (2014), 103514.
[27] Z. Zeng, X. Ma, J. Chen, Y. Zeng, D. Yang, Y. Liu, J. Appl. Phys. 107 (12) (2010), 123503.
[28] F. Birch, J. Geophys. Res. 57 (2) (1952) 227–286.
[29] B. Bhushan, X. Li, J. Mater. Res. 12 (1) (1997) 54–63.
[30] C.S. Oh, H.J. Lee, S.G. Ko, S.W. Kim, H.G. Ahn, Sens. Actuator A Phys. 117 (1) (2005) 151–158.
[31] R.F. Cook, J. Mater. Sci. 41 (3) (2006) 841–872.
[32] W.N. Sharpe, Y. Bin, R. Vaidyanathan, R.L. Edwards, Measurements of Young's modulus, Poisson's ratio, and tensile strength of polysilicon, in: Proceedings IEEE The Tenth Annual International Workshop on Micro Electro Mechanical Systems. An Investigation of Micro Structures, Sensors, Actuators, Machines and Robots, 1997, pp. 424–429.
[33] S. Anzellini, M.T. Wharmby, F. Miozzi, A. Kleppe, D. Daisenberger, H. Wilhelm, Sci. Rep. 9 (1) (2019) 15537.
[34] J.G. Swadener, M. Nastasi, J. Mater. Sci. Lett. 21 (17) (2002) 1363–1365.
[35] H.S. Kim, M.B. Bush, Nanostruct. Mater. 11 (3) (1999) 361–367.

[36] Z. Zeng, Q. Zeng, M. Ge, B. Chen, H. Lou, X. Chen, J. Yan, W. Yang, H.K. Mao, D. Yang, W.L. Mao, Phys. Rev. Lett. 124 (18) (2020), 185701.
[37] A.P. Gerk, D. Tabor, Nature 271 (1978) 732–733.
[38] G.M. Pharr, W.C. Oliver, D.R. Clarke, J. Electron. Mater. 19 (9) (1990) 881–887.